Efficient MPIE Approach for the Analysis of Three-Dimensional Microstrip Structures in Layered Media

Rainer Bunger, *Member, IEEE,* and Fritz Arndt, *Fellow, IEEE*

***Abstract*— A full-wave space-domain method is presented for the rigorous and fast investigation of printed circuit structures of arbitrary shape on uniaxial anisotropic layered substrates including three-dimensional (3-D) metallizations. The electromagnetic (EM) fields are described in terms of a mixed-potential-integral-equation (MPIE) formulation. Two different techniques—the matrix pencil (MP) technique and a cross-sectional eigenvalue (CSEV) approach—are employed to extract the S-parameters of the circuit under consideration. The usage of a triangular mesh allows the convenient modeling of arbitrarily shaped structures. Therefore, the main advantage of this method is its generality, which allows a large variety of printed circuit structures to be characterized. The flexibility of the method is demonstrated at the example of spiral inductors including air-bridges with finite-metallization thickness.**

I. Introduction

VERTICAL interconnect elements in multilayered circuit environments, such as air-bridges, via holes, or bond-wires, play a significant role in recent microwave monolithic integrated circuit (MMIC) technology [2], [10], [19], [21]. Up to now, for the full-wave analysis of such three-dimensional (3-D) structures, the spectral-domain-analysis (SDA) technique [2], the finite-difference time-domain (FDTD), finite-element (FE) (e.g., [10], [21]), and mode-matching (MM) methods [19] have been applied. Although very flexible, the numerical FDTD or FE approaches require a significant effort in central processing unit (CPU) time and storage requirements. The extensive use of the fast Fourier transform (FFT) algorithm makes the SDA technique very efficient, but limits, on the other side, its application to structures with identical segment sizes. The MM technique in [19] is restricted to rectangular via holes. It may, therefore, be desirable to dispose of adequate analysis and circuit design techniques for 3-D passive MMIC devices, which combine the advantage of full flexibility with that of numerical efficiency.

In this paper, a flexible full-wave space-domain mixed-potential-equation (MPIE) method is described for the rigorous and fast investigation of printed circuit structures of arbitrary shape on layered substrates including 3-D metallizations. Up to now, for MMIC structures, the MPIE approach has been used merely for planar two-dimensional (2-D) printed circuits [9]. A triangular mesh allows the convenient modeling of arbitrarily shaped structures without the assumption of specific attachment basis functions. Although the usage of a wire model may be adequate for the modeling of vias, coax pins, and thin bond wires, this approach would be inaccurate for air-bridges used in MMIC devices.

The space-domain technique has already been successfully applied at scattering problems [13]. The efficiency of the MPIE formulation is demonstrated in [13] at the example of the dielectric half-space where computationally efficient expressions for the Sommerfeld-type integrals have been introduced. In this paper, in order to maintain the full flexibility of the space-domain method, no special assumptions are made.

The matrix pencil (MP) technique [7], [8] and a cross-sectional eigenvalue (CSEV) approach are employed to extract the S-parameters of the circuit under consideration. By contrast with the MP technique, the CSEV approach turns out to also yield accurate results for very short port-line lengths. The efficiency of the presented method is demonstrated within the example of spiral inductors including air-bridges (Fig. 1). For the rectangular structure [Fig. 1(a)], the available reference values in [2] for negligible metallization thickness of the air-bridge are used to verify these results. Moreover, the authors' FDTD calculations are carried out for reference purposes. In contrast to [2], in this paper the air-bridges may include finite-metallization thicknesses (Fig. 1).

II. Theory

A. Formulation of the MPIE

The Green's functions for the mixed potentials have already been derived by Michalski and Zheng in [11]–[13]. Therefore, only a short summary will be given here, concentrating mainly on new aspects. For further details of the basic theory, the reader is referred to the literature.

The boundary condition for the electric field on the S surface of the perfect metallic scatterer is

$$-\hat{\boldsymbol{n}} \times \boldsymbol{E}^{sc}(\boldsymbol{r}) = \hat{\boldsymbol{n}} \times \boldsymbol{E}^{\text{inc}}(\boldsymbol{r}), \qquad \boldsymbol{r} \text{ on } S. \tag{1}$$

$\hat{\boldsymbol{n}}$ is the unit normal vector of the scatterers surface S. $\boldsymbol{E}^{\text{inc}}$ and $\boldsymbol{E}^{sc}$ are the incident and scattered fields in complex notation. The mixed-potential-integral equation (MPIE) is written as

$$-\boldsymbol{E}^{sc}(\boldsymbol{r}) = j\omega \boldsymbol{A}(\boldsymbol{r}) + \nabla\phi(\boldsymbol{r}) \tag{2}$$

using the vector potential

$$\boldsymbol{A}(\boldsymbol{r}) = \int_S \boldsymbol{\mathcal{G}}^A(\boldsymbol{r}, \boldsymbol{r}') \cdot \boldsymbol{J}_S(\boldsymbol{r}')\, dS' \tag{3}$$

Manuscript received June 11, 1995; revised April 25, 1997.

The authors are with the Microwave Department, University of Bremen, D-28334 Bremen, Germany.

Publisher Item Identifier S 0018-9480(97)05368-4.

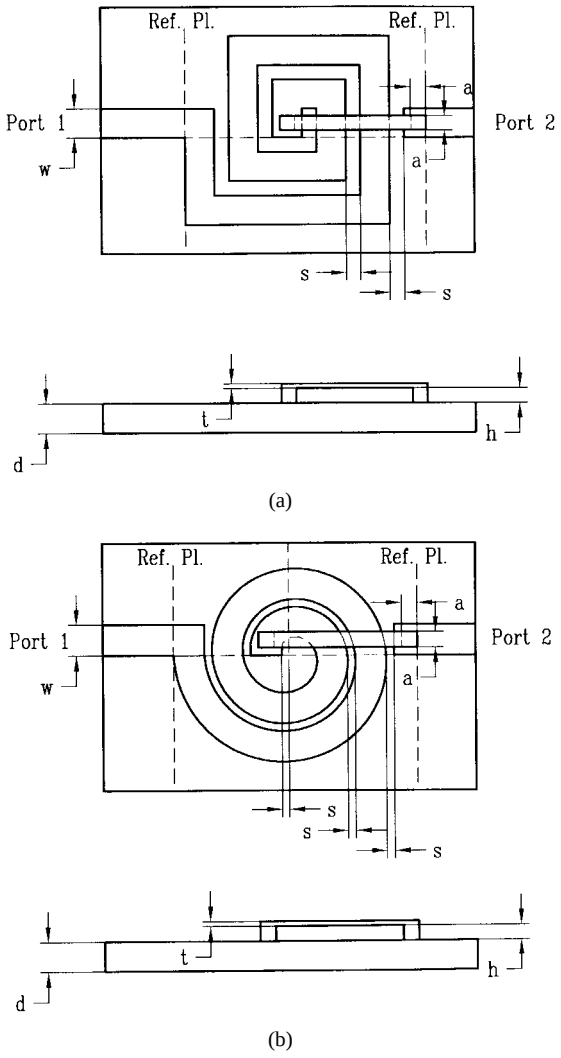

Fig. 1. Spiral inductors in microstrip technique with an air-bridge of finite-metallization thickness. (a) Rectangular spiral and (b) continuous spiral structures. Dimensions for the rectangular structure analogous to [2]: $a = s = 0.3125$ mm, $w = 0.625$ mm, $h = 0.3175$ mm, $d = 0.635$ mm, $\epsilon_r = 9.8$, $\tan\delta = 0$. Here, $t \neq 0$.

and the scalar potential

$$\phi(\boldsymbol{r}) = \int_S G^{\phi}(\boldsymbol{r}, \boldsymbol{r}')\, q_S(\boldsymbol{r}')\, dS' \tag{4}$$

where the surface–current density is related to the surface-charge density by

$$\nabla'_S \cdot \boldsymbol{J}_S(\boldsymbol{r}') + j\omega q_S(\boldsymbol{r}') = 0. \tag{5}$$

$\boldsymbol{\mathcal{G}}^A$ and G^{ϕ} are dyadic and scalar Green's functions for the vector and scalar potential.

B. Green's functions

The Green's functions for the scalar and vector potential may be derived from the Green's function $\boldsymbol{\mathcal{G}}^{EJ}$ for the electric field produced by an electric source. Because of the fact that the relation between the Green's functions for the electric field and the mixed potentials is not unique, different formulations are possible. Michalski and Zheng [11], [12] have discussed in detail three formulations. Their formulation C results in a continuous function G^{ϕ}.

The derivation of $\boldsymbol{\mathcal{G}}^{EJ}$ in this paper is based on a formulation by Felsen in [3]. This formulation relates the Green's functions $\boldsymbol{\mathcal{G}}^{EJ}$ for the fields to the transmission-line Green's functions, T, Y, Z [3], and allows a high flexibility of the MPIE technique. Since the equations in [3] are given for source-free regions, an extension for source regions is necessary.

To clarify some notations, the observation point residing in the ith layer is denoted by (x, y, z) and the source point residing in the jth layer is denoted by (x', y', z'), respectively. The generally uniaxial anisotropic layered medium of infinite extend in the x- and y-directions is characterized by the relative permittivity and permeability dyadics

$$\boldsymbol{\epsilon}^i_r = (\hat{\boldsymbol{x}}\hat{\boldsymbol{x}} + \hat{\boldsymbol{y}}\hat{\boldsymbol{y}})\epsilon^i_{rt} + \hat{\boldsymbol{z}}\hat{\boldsymbol{z}}\epsilon^i_{rz} \tag{6}$$

$$\boldsymbol{\mu}^i_r = (\hat{\boldsymbol{x}}\hat{\boldsymbol{x}} + \hat{\boldsymbol{y}}\hat{\boldsymbol{y}})\mu^i_{rt} + \hat{\boldsymbol{z}}\hat{\boldsymbol{z}}\mu^i_{rz} \tag{7}$$

for the ith layer. Using the notation of Felsen in [3] for the transmission-line Green's functions T, Y, Z,[1] one obtains for the dyadic and scalar Green's functions

$$\begin{aligned}
j\omega\boldsymbol{\mathcal{G}}^A(\varrho, z, z') &= (\hat{\boldsymbol{x}}\hat{\boldsymbol{x}} + \hat{\boldsymbol{y}}\hat{\boldsymbol{y}})\,\mathcal{S}_0\{Z''(z, z')\} \\
&\quad - \hat{\boldsymbol{z}}\hat{\boldsymbol{x}}\cos\varphi\, jk_0\eta_0\mu^i_{rt}\,\mathcal{S}_1\left\{\frac{T''^I(z, z') - T'^I(z, z')}{k_\varrho^2}\right\} \\
&\quad - \hat{\boldsymbol{z}}\hat{\boldsymbol{y}}\sin\varphi\, jk_0\eta_0\mu^i_{rt}\,\mathcal{S}_1\left\{\frac{T''^I(z, z') - T'^I(z, z')}{k_\varrho^2}\right\} \\
&\quad - \hat{\boldsymbol{x}}\hat{\boldsymbol{z}}\cos\varphi\, jk_0\eta_0\mu^j_{rt}\,\mathcal{S}_1\left\{\frac{T''^V(z, z') - T'^V(z, z')}{k_\varrho^2}\right\} \\
&\quad - \hat{\boldsymbol{y}}\hat{\boldsymbol{z}}\sin\varphi\, jk_0\eta_0\mu^j_{rt}\,\mathcal{S}_1\left\{\frac{T''^V(z, z') - T'^V(z, z')}{k_\varrho^2}\right\} \\
&\quad + \hat{\boldsymbol{z}}\hat{\boldsymbol{z}}\eta_0^2\mu^i_{rt}\mu^j_{rt}\,\mathcal{S}_0\left\{\left(\frac{k_0}{k_\varrho}\right)^2 Y''(z, z') \right. \\
&\quad \left. + \left[\frac{1}{\mu^i_{rt}\epsilon^i_{rz}} + \frac{1}{\mu^j_{rt}\epsilon^j_{rz}} - \left(\frac{k_0}{k_\varrho}\right)^2\right] Y'(z, z')\right\}
\end{aligned} \tag{8}$$

$$-\frac{1}{j\omega}\,G^{\phi}(\boldsymbol{\varrho}, z, z') = \mathcal{S}_0\left\{\frac{Z''(z, z') - Z'(z, z')}{k_\varrho^2}\right\} \tag{9}$$

with

$$\begin{aligned}
\boldsymbol{\varrho} &= \hat{\boldsymbol{x}}(x - x') + \hat{\boldsymbol{y}}(y - y') \\
&= \varrho(\hat{\boldsymbol{x}}\cos\varphi + \hat{\boldsymbol{y}}\sin\varphi).
\end{aligned} \tag{10}$$

Like formulation C in [11], this results in a continuous function G^{ϕ}, so that no additional contour integrals in the space domain are needed. The definition of the Sommerfeld integral $\mathcal{S}_n$, as well as the relations for the transmission-line Green's functions T, Z, Y, are given in the Appendix.

[1] According to [3], the superscript $''$ denotes H-waves, and the superscript $'$ denotes E-waves.

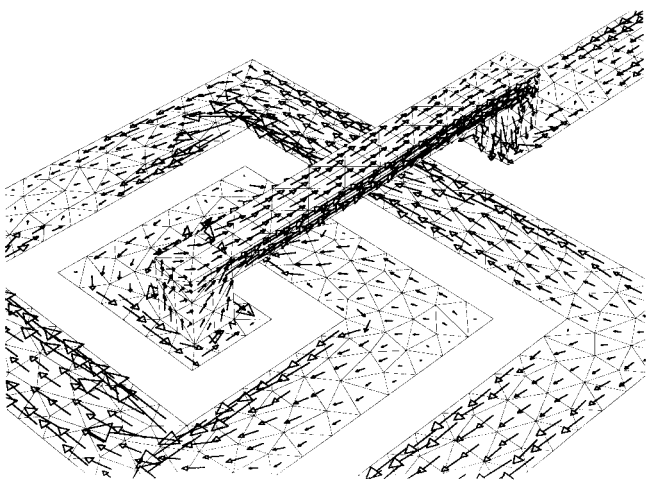

Fig. 2. Real part of the surface–current distribution on the metallic surface of the rectangular spiral inductor [Fig. 1(a)], $t = 0.156\,25$ mm, $f = 11$ GHz. Also shown is the triangular mesh.

C. Method of Moments

For the solution of the MPIE, the method of moments (MoM) with triangular patches (see Fig. 2) and a set of basis functions as described in [17] are used. Additional attachment basis functions near the attachment points of coax pins or wires [22] preserve the continuity of the current at the junctions.

The ordinary basis function belonging to a common edge n of two triangles T_n^+ and T_n^- is defined as

$$\boldsymbol{f}_n(\boldsymbol{r}) = \begin{cases} \dfrac{\boldsymbol{\varrho}_n^+(\boldsymbol{r})}{2A_n^+}, & \boldsymbol{r} \text{ in } T_n^+ \\ \dfrac{\boldsymbol{\varrho}_n^-(\boldsymbol{r})}{2A_n^-}, & \boldsymbol{r} \text{ in } T_n^- \\ \boldsymbol{0}, & \text{otherwise.} \end{cases} \tag{11}$$

The $A_n^\pm$ are the areas of the triangles $T_n^\pm$. The vectors $\boldsymbol{\varrho}_n^\pm(\boldsymbol{r})$ are defined as $\pm(\boldsymbol{r} - \boldsymbol{r}_n^\pm)$ if $\boldsymbol{r}$ is in $T_n^\pm$, where the vectors $\boldsymbol{r}_n^\pm$ are the position vectors of the free vertices of the triangle pair.

The attachment basis function used here is the *simplified-attachment basis function* presented in [22]. Considering a single attachment point, there are Q^A triangles q connected to it, where one of the vertices must be the attachment point. If the three vertices of a triangle q are denoted with i, j, and k, and their opposite edges with the vectors $\boldsymbol{l}_q^i$, $\boldsymbol{l}_q^j$, and $\boldsymbol{l}_q^k$, then vertex j shall be the attachment point. The angle between the edges $\boldsymbol{l}_q^i$ and $\boldsymbol{l}_q^k$ is α_q^j, the total angle α is defined for each attachment point as the sum of all its angles α_q^j. Using this notation, the first part of the attachment basis functions on the attached triangles can be written as

$$\boldsymbol{f}_n(\boldsymbol{r}) = -\sum_{q=1}^{Q^A} \frac{\alpha_q^j}{2\alpha} \left[\frac{\boldsymbol{\varrho}_q^i(\boldsymbol{r})}{2A_q} + \frac{\boldsymbol{\varrho}_q^k(\boldsymbol{r})}{2A_q} \right] \tag{12}$$

with

$$\boldsymbol{\varrho}_q^i(\boldsymbol{r}) = \begin{cases} \boldsymbol{r} - \boldsymbol{r}_q^i, & \boldsymbol{r} \text{ in } T_q \\ \boldsymbol{0}, & \text{otherwise} \end{cases} \tag{13}$$

where $\boldsymbol{r}_q^i$ is the position vector to the vertex i of triangle q, and A_q is the area of triangle q. On the attached wire segment, the current is modeled with a semirooftop function with the maximum on the attachment point. This is the second part of the attachment basis function.

Introducing the approximation

$$\boldsymbol{J}_S(\boldsymbol{r}) \approx \sum_{n=1}^{N} I_n \boldsymbol{f}_n(\boldsymbol{r}) \tag{14}$$

for the surface–current density on S, using Galerkin's method, and applying the 2-D divergence theorem, yields for the mth equation

$$\sum_{n=1}^{N} I_n \left\{ j\omega \int_S \boldsymbol{f}_m(\boldsymbol{r}) \cdot \boldsymbol{A}_n(\boldsymbol{r})\, dS - \int_S [\nabla_S \cdot \boldsymbol{f}_m(\boldsymbol{r})] \phi_n(\boldsymbol{r})\, dS \right\} = \int_S \boldsymbol{f}_m(\boldsymbol{r}) \cdot \boldsymbol{E}^{\text{inc}}(\boldsymbol{r})\, dS \tag{15}$$

where the potentials are defined as

$$\boldsymbol{A}_n(\boldsymbol{r}) = \int_{T_n^+ + T_n^-} \boldsymbol{\mathcal{G}}^A(\boldsymbol{r}, \boldsymbol{r}') \cdot \boldsymbol{f}_n(\boldsymbol{r}')\, dS' \tag{16}$$

and

$$\phi_n(\boldsymbol{r}) = -\frac{1}{j\omega} \int_{T_n^+ + T_n^-} G^\phi(\boldsymbol{r}, \boldsymbol{r}') \nabla'_S \cdot \boldsymbol{f}_n(\boldsymbol{r}')\, dS'. \tag{17}$$

The system matrix of the resulting linear system of equations is called *impedance matrix*, the right-hand side (RHS) vector is called *excitation* or *voltage* vector.

The first part of the simplified-attachment basis function, which is defined on the attached triangles with a prescribed amplitude, may be used as the source for the incident field $\boldsymbol{E}^{\text{inc}}$. This is a good choice for the excitation if scattering parameters related to microstrip lines are computed.[2] The algebraic and the computational effort for the calculation of the excitation vector is negligible as it is computed in the same way as the impedance matrix. However, if scattering parameters related to coaxial cables are of interest, the coax pins should be included into the integral equation. In this case, the magnetic-current frill excitation is an accurate source for the incident field [22].

D. Extraction of the Scattering Parameters

For the determination of the scattering matrix of the N-port structure, the incident and reflected fundamental modes on the N microstrip lines must be known for N different excitations.[3] The resulting linear system of equations $\boldsymbol{B} = \boldsymbol{S} \cdot \boldsymbol{A}$, where $\boldsymbol{A}$ and $\boldsymbol{B}$ are $N \times N$ matrices of the N vectors $\boldsymbol{a}$ and $\boldsymbol{b}$ for the N different excitations is solved for the scattering matrix $\boldsymbol{S}$. The fundamental modes and even higher order modes on the microstrip lines are determined by utilization of the efficient MP technique, which is discussed in detail in [7] and [8].

The MP technique is used advantageously for the estimation of parameters of complex exponentials in noise. The efficiency of the MP technique results, in particular, from the fact that an eigenvalue problem can be formulated for the determination

[2] In this case, the attachment function is not a "basis" function in the original sense and is not included in the set of the N basis functions.

[3] Here, N denotes the number of transmission lines.

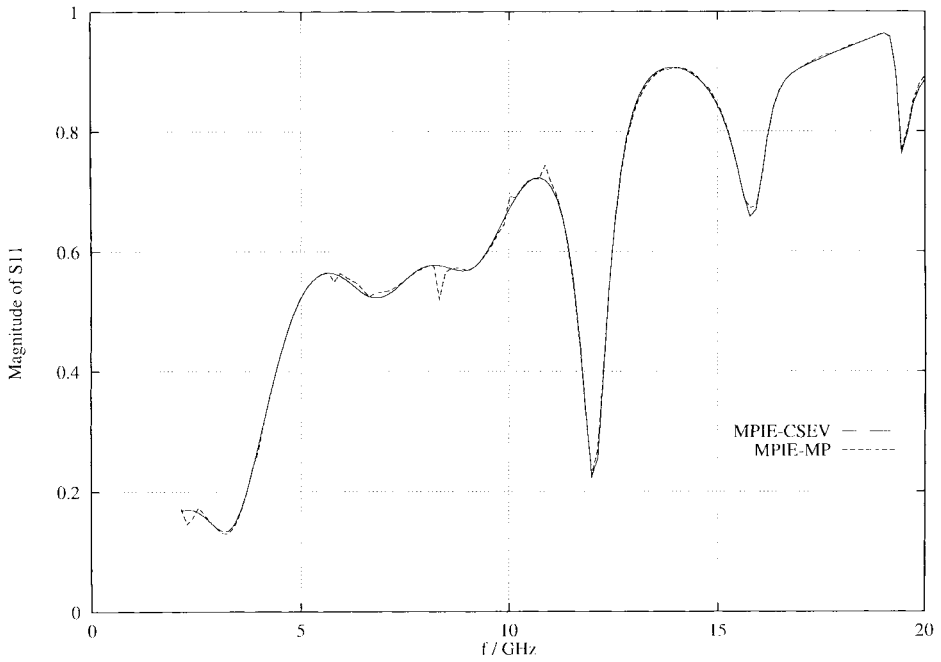

(a)

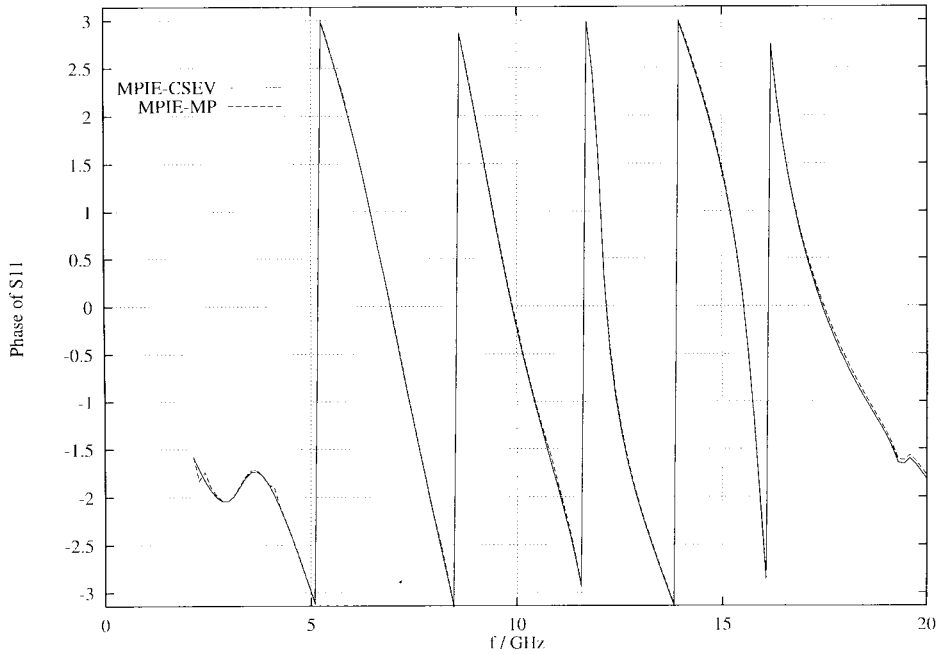

(b)

Fig. 3. Comparison of two different methods, the MP technique and the CSEV approach, for the scattering parameter extraction $t = 0$. (a) S_{11}, magnitude, 10-mm line length. (b) S_{11}, phase, 10-mm line length.

of the signal poles. The sampled data sequence of length K is described by

$$y_k = \sum_{t=1}^{M} b_t e^{(\alpha_t + j\beta_t)k} + n_k = \sum_{t=1}^{M} b_t z_t^k + n_k \tag{18}$$

where n_k denotes the noise, z_t the signal poles, and $k = 0, 1, \cdots, K-1$. It can be shown [7] that the signal poles can be estimated by the generalized eigenvalues of a *matrix pencil* (*MP*)

$$\boldsymbol{Y}_1 - z\boldsymbol{Y}_2 \tag{19}$$

where $\boldsymbol{Y}_1$ and $\boldsymbol{Y}_2$ are data matrices, as described in [7]. The utilization of singular-value decomposition techniques leads to a stable approximation of the matrix pencil, and the signal poles are computed as its eigenvalues. If all z_t are known, the residues b_t are obtained after a solution of an overdetermined linear system of equations by a singular-value decomposition in the least square sense.

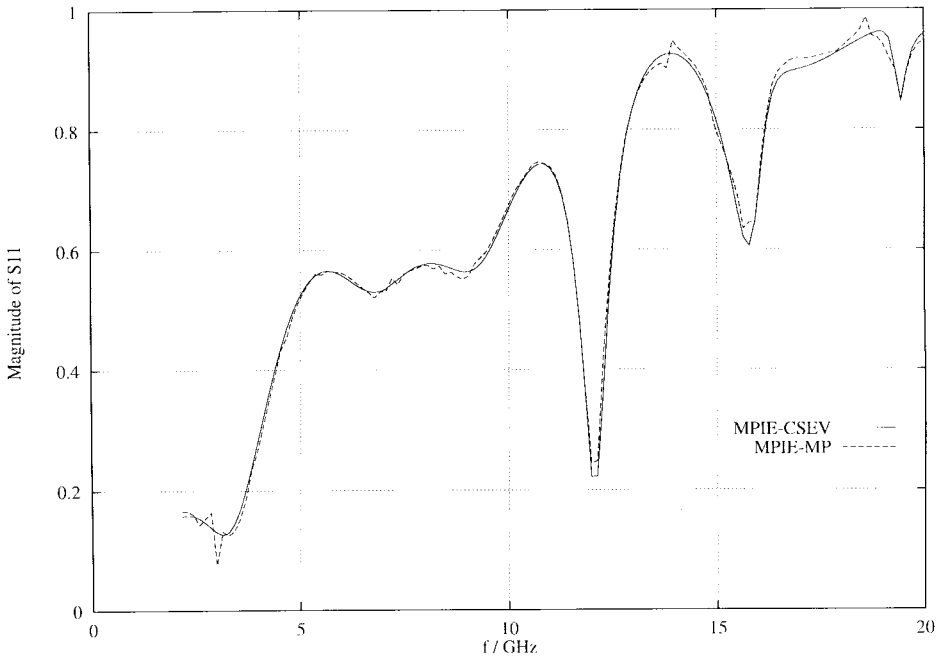

(c)

Fig. 3. *(Continued.)* Comparison of two different methods, the MP technique and the CSEV approach, for the scattering parameter extraction $t = 0$. (c) S_{11}, magnitude, 5-mm line length.

For the determination of the matrices $\boldsymbol{A}$ and $\boldsymbol{B}$, the line currents on the N microstrip lines are sampled for each of the N excitations. From these line currents, all desired modes can be extracted with the help of the MP technique.

A second technique is based on the CSEV's. An adequate technique for the analysis of the cross section problem of transmission lines in multilayered media, like that described in [6], may be used to compute the surface–current eigenmodes. From these modes, the characteristic impedance of the fundamental mode may be computed most easily using the voltage–current definition. The generally preferred power–current definition requires the integration of the Poynting vector in the transversal xz cross section of the transmission line, where the integration over the horizontal variable x can be transformed into an integration over the corresponding spectral wavenumber k_x [16]. In this paper, the voltage–current definition of the characteristic impedance has been used.

It is also possible to use not only the characteristic impedance of the eigenmodes but also the eigenvalues and eigenmodes itself for the extraction of the scattering parameters. The computed surface–current distribution on the transmission lines of the investigated 3-D structure may be expressed by a weighted sum of eigenmodes with unknown amplitudes. The resulting equation, which relates the eigenmode expansion of the surface current to the computed surface current, is tested with the eigenmodes, and a linear system of equations for the expansion coefficients is obtained. These coefficients are used as described above to compute the scattering parameters.

In the present context, only a single eigenmode (for each direction) has been used in order to extract the scattering parameters.

III. Numerical Implementation

A. Treatment of Green's Functions Static Parts

The static parts of the Green's functions in the spectral domain are the asymptotic terms for $k_\varrho \to \infty$, where k_ϱ is the spectral variable. In the space domain, the static parts are the singular parts of Green's functions. Therefore, the extraction of the static parts from the Sommerfeld integral integrands increases the convergence of the Sommerfeld integrals and yields regular results in the space domain. The extracted static parts in the spectral domain are transformed into the space domain analytically by using the Sommerfeld identity

$$\int_C J_0(k_\varrho \varrho) \frac{e^{-jk_z|z|}}{jk_z} k_\varrho \, dk_\varrho = \frac{e^{-jkr}}{r} \tag{20}$$

where C is a path from 0 to ∞, and the relation

$$\int_C J_1(k_\varrho \varrho) e^{-jk_z|z|} \, dk_\varrho = \frac{e^{-jkr}}{\varrho} - \frac{|z|}{\varrho r} e^{-jkr} \tag{21}$$

which may be derived by integration by parts.

When source and observation points are located in the same layer, the first three largest asymptotic terms are extracted in the spectral domain. In the space domain, these three static terms represent the *direct* part, and two *images* at the upper and lower interfaces. In this way, the Sommerfeld integrals yield very smooth results in the space domain. When source and observation points are located in different, but neighboring, layers, only the largest asymptotic terms are extracted. In this case, there are no *image* terms. The *direct* and *image* parts can be identified directly from the transmission-line Green's functions.

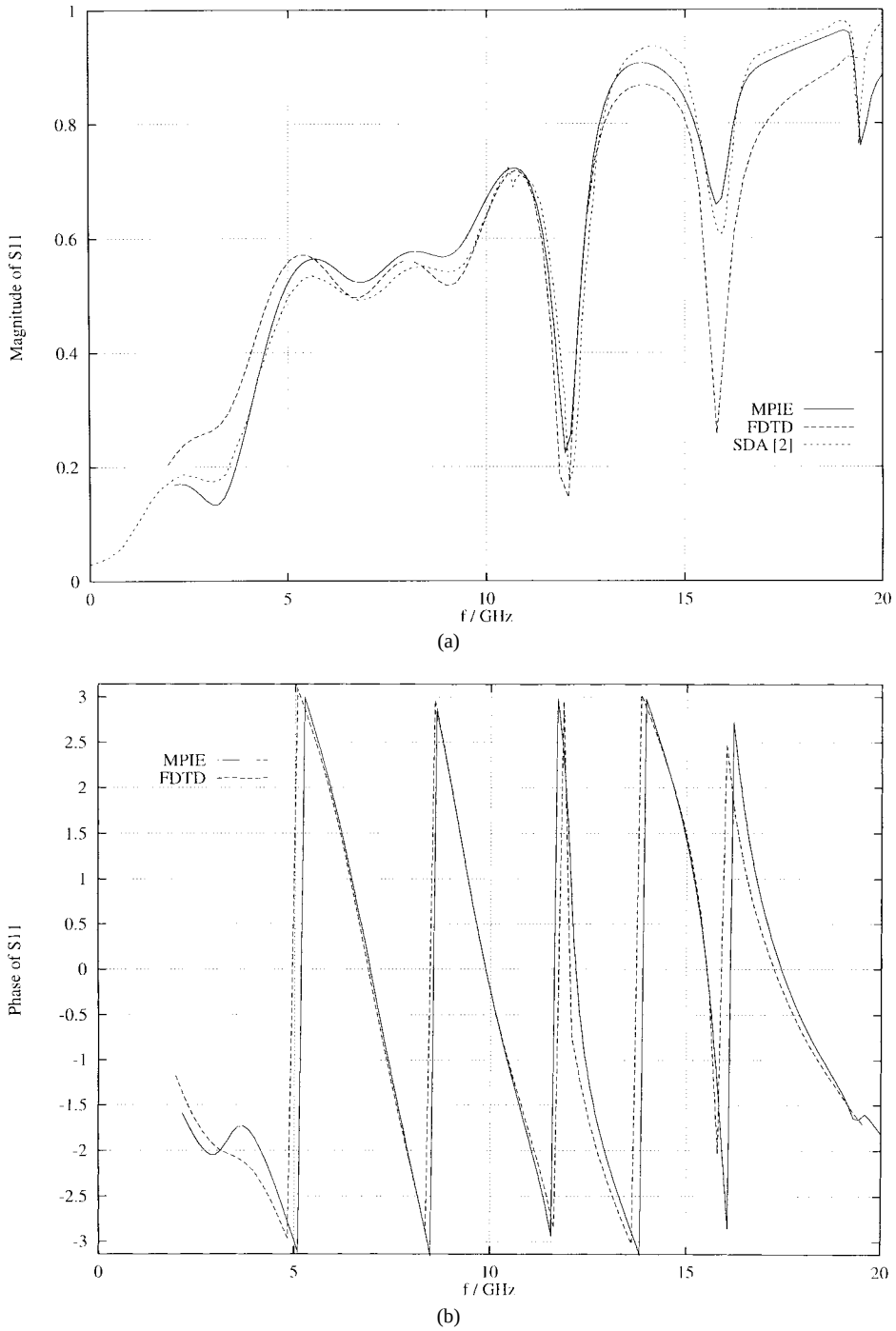

Fig. 4. Magnitude and phase of the S-parameters of the structure of Fig. 1 for $t = 0$. Comparison with the SDA [2] and the authors' FDTD calculations. (a) S_{11}, magnitude and (b) S_{11}, phase.

ACKNOWLEDGMENT

Dealing with G^{ϕ} and the diagonal elements of $\mathcal{G}^{A}$ for the calculation of the scalar and vector potentials, (16) and (17), one to three static parts are integrated for the scalar potential, and one up to three static parts are integrated (multiplied with the basis function) for the diagonal elements of $\mathcal{G}^{A}$ for the vector potential using the equations developed in [20]. For the nondiagonal elements of $\mathcal{G}^{A}$, the analytical expressions of the extracted static parts are singular only at the interfaces between the adjacent layers. Since the terms of the static parts multiplied with the basis functions cannot be integrated analytically, the static parts are simply added to the nondiagonal regular parts of $\mathcal{G}^{A}$ in the space domain, and integrated numerically. The singularity of the total nondiagonal elements of $\mathcal{G}^{A}$ poses no numerical difficulties, because the triangular segments are not allowed to cross the interface between adjacent layers.

The treatment of the singularities in layered media is similar to the treatment of singularities in free space, the only difference is the appearance of additional *image* terms.

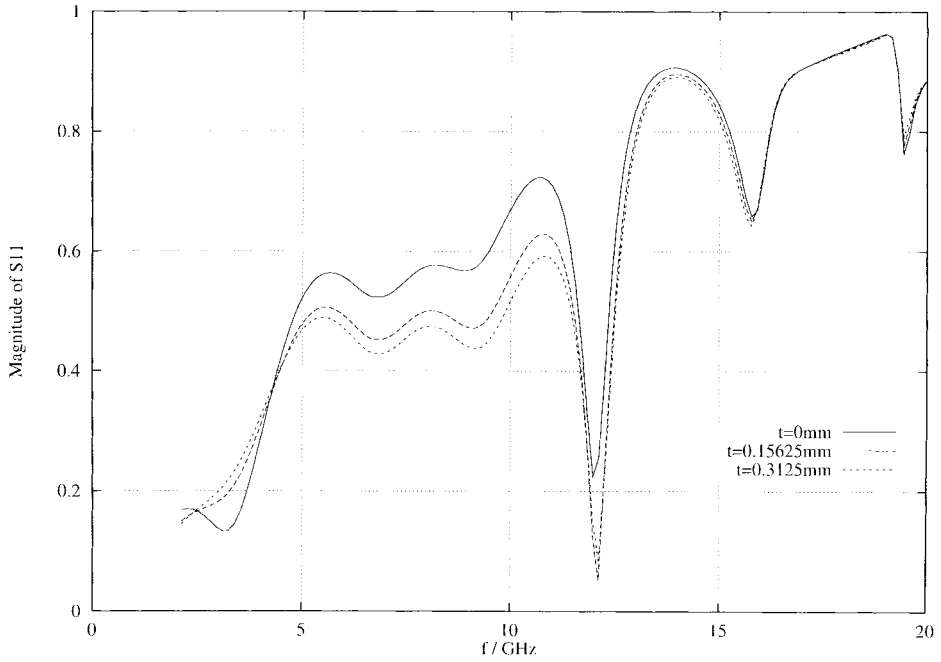

(a)

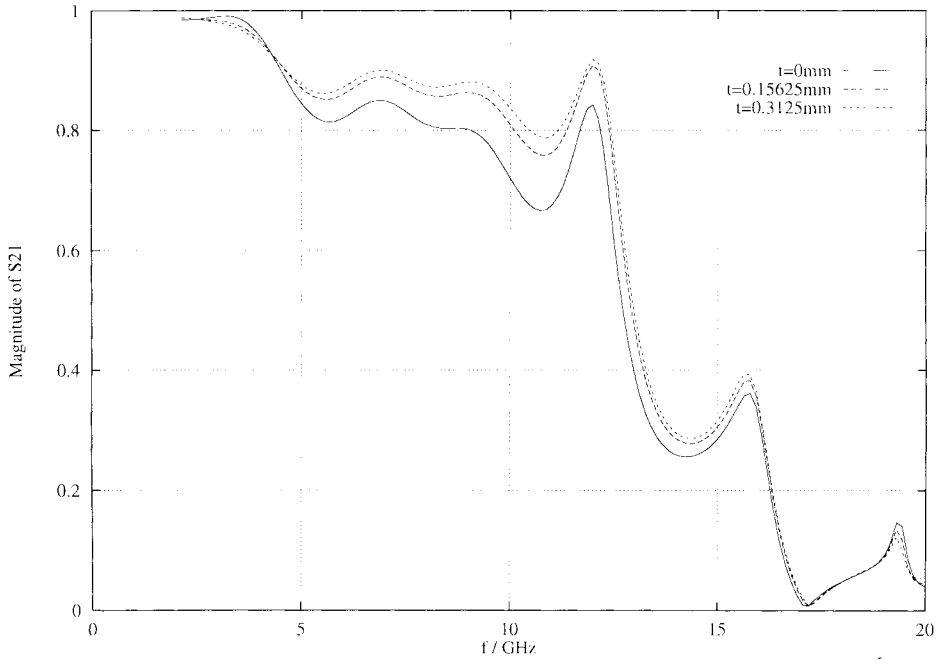

(b)

Fig. 5. Influence of the finite thickness t of the air-bridge on the magnitude and phase of the scattering parameters. (a) S_{11}, magnitude and (b) S_{21}, magnitude.

B. Evaluation of the Sommerfeld Integrals

For the integration in the complex k_ϱ-plane along the real axis only, Mosig [14], [15] has proposed some techniques for the efficient numerical integration near the surface poles and the branch cut. The pole-extraction technique would work well for special applications, but in general, the number of poles is not known, and, hence, the extraction of the poles is difficult in this case.

Therefore, a different integration path (partially above the real axis) has been chosen. The integral is computed along 0 to $0.25k_0 + j0.25k_0$, to $\max(\mathrm{Re}\sqrt{k_0\epsilon^i_{\mathrm{rt}}\mu^i_{\mathrm{rt}}}) + j0.25k_0$, and back to $\max(\mathrm{Re}\sqrt{k_0\epsilon^i_{\mathrm{rt}}\mu^i_{\mathrm{rt}}}) + 0.25k_0$ for the first interval. This path works even if parallel-plate poles must be considered.

For the subsequent real-axis integration up to infinity, Mosig's method of averages [14] is considered to be the best choice. The convergence of this technique is very fast.

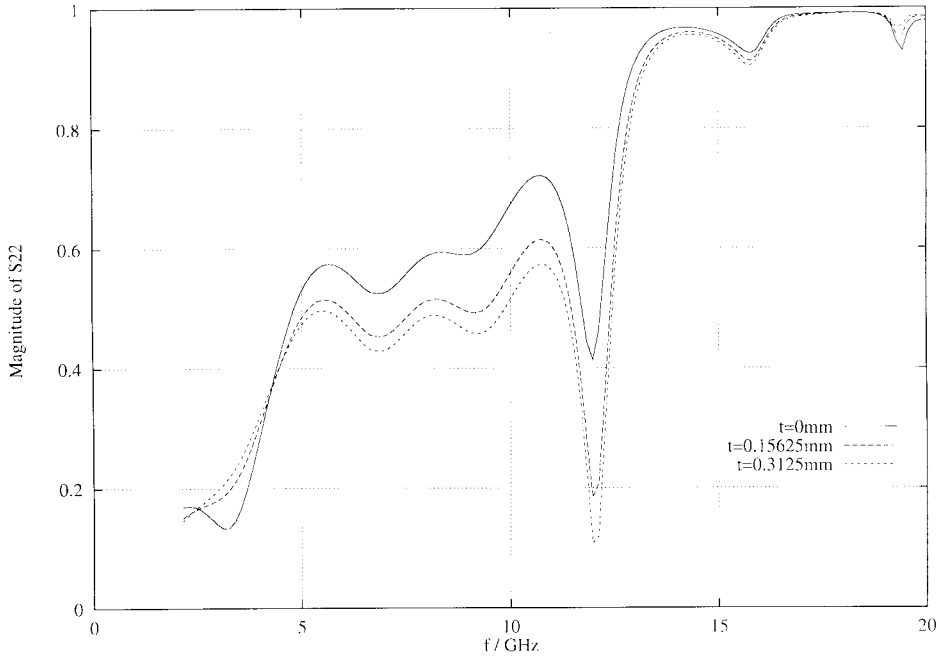

(c)

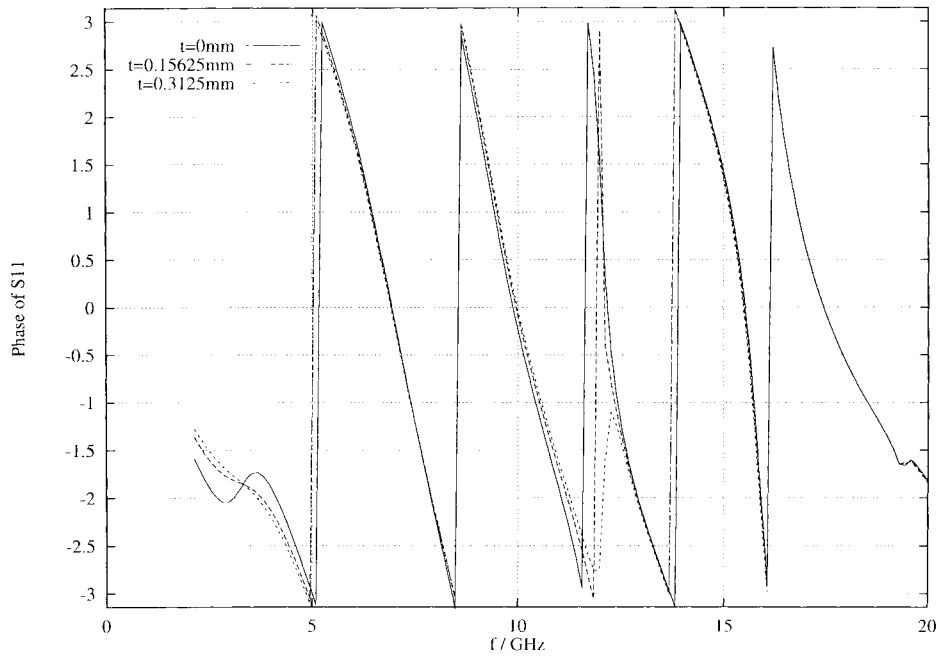

(d)

Fig. 5. *(Continued.)* Influence of the finite thickness t of the air-bridge on the magnitude and phase of the scattering parameters. (c) S_{22}, magnitude and (d) S_{11}, phase.

A further improvement of the convergence rate is obtained after the extraction of static parts, as discussed in Section III-A.

C. Interpolation of Green's Functions

Usual interpolation techniques (over ϱ) for planar scattering problems are known to work very well. However, for this paper's 3-D scattering problem in layered media, a 3-D interpolation (over ϱ, z, and z') is required, and very smooth functions are necessary. Fortunately, the Green's functions without the (extracted) static terms are sufficiently regular, and only a few sampling points are necessary in the z-direction. Therefore, the memory and time requirements for this 3-D interpolation are very low. A Lagrange interpolation of the second degree has been used here.

D. Determination of the Linear System of Equations

The procedure for the computation of the impedance matrix elements is based on the technique of [17]. The testing integral is calculated using a one-point integration rule (i.e., one-point

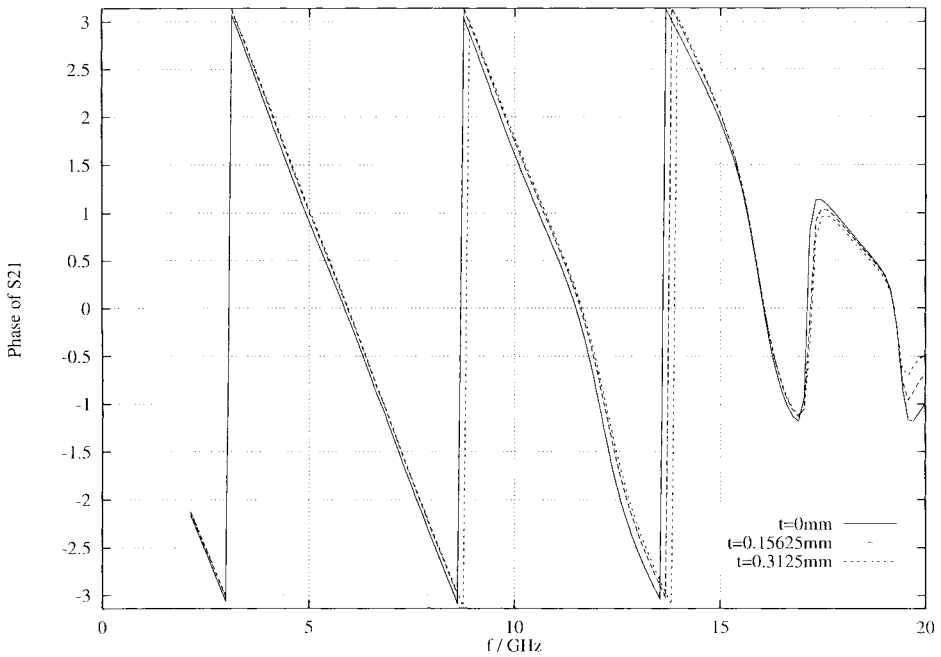

(e)

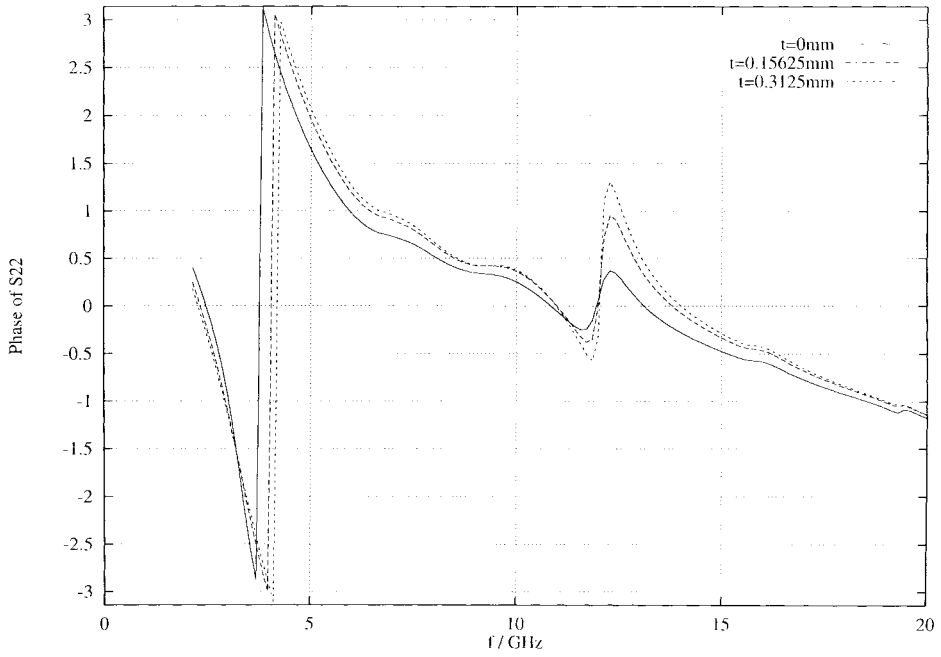

(f)

Fig. 5. *(Continued.)* Influence of the finite thickness t of the air-bridge on the magnitude and phase of the scattering parameters. (e) S_{21}, phase and (f) S_{22}, phase.

testing procedure) as a special case of a numerical low-order integration. The error of the computed surface currents obtained by this rather coarse approximation turned out to be very small. Exceptions are microstrip antennas near a resonance frequency, where a three-point test integration rule may be used.

For the efficient computation of the impedance matrix and excitation vector elements, an adequate preprocessing technique is important after the generation of the triangular mesh. Although the ordinary basis functions are assigned to internal edges, it would not be efficient to utilize a nested loop procedure for the observation and source-basis functions m and n. An efficient algorithm, however, is obtained by introducing the potentials

$$\boldsymbol{A}_q^j(\boldsymbol{r}) = \int_{T_q} \boldsymbol{\mathcal{G}}^A(\boldsymbol{r}, \boldsymbol{r}') \cdot \boldsymbol{\varrho}_q^j(\boldsymbol{r}')\, dS' \tag{22}$$

and

$$\phi_q^j = -\frac{1}{j\omega} \int_{T_q} G^\phi(\boldsymbol{r}, \boldsymbol{r}')\, dS' \tag{23}$$

where $j = 1, \cdots, 3$ denotes the vertices of a source trian-

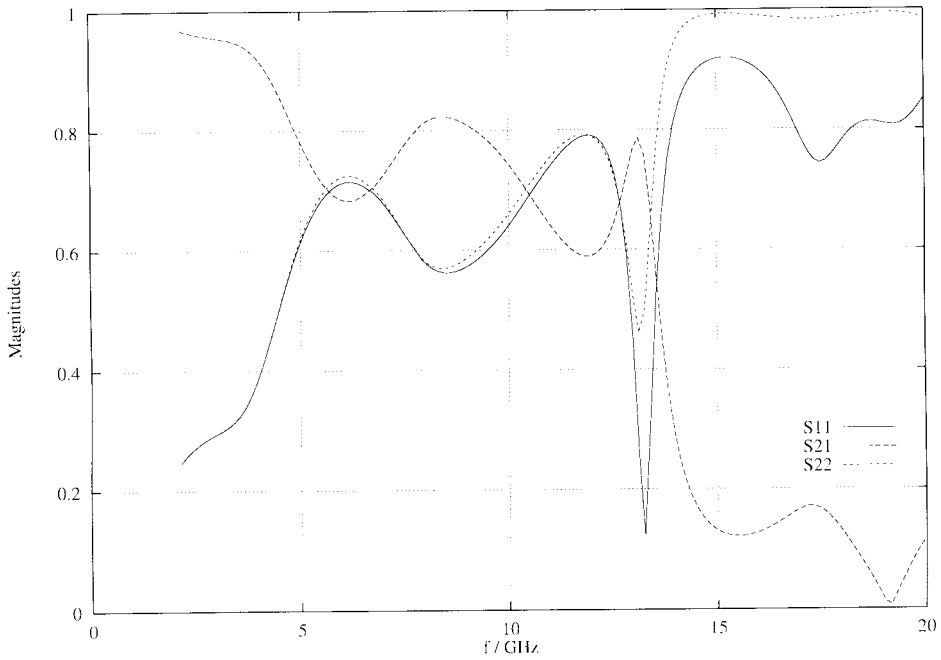

(a)

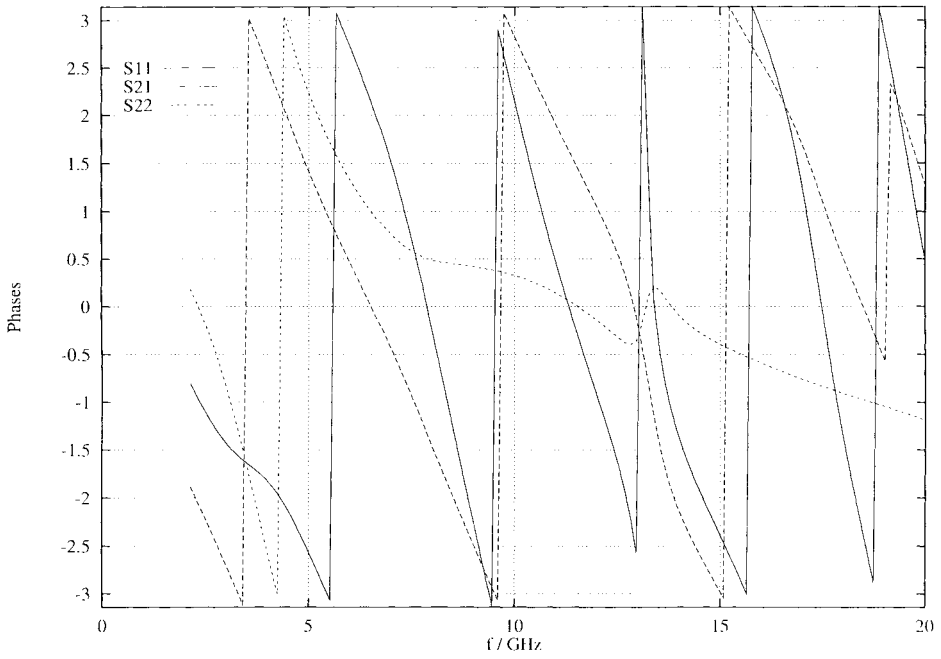

(b)

Fig. 6. Scattering parameters of the continuous spiral inductor of Fig. 1(b). Dimensions: $a = 0.3125$ mm, $s = 0.15625$ mm, $w = 0.625$ mm, $h = 0.3175$ mm, $d = 0.635$ mm, $\epsilon_r = 9.8$, $\tan\delta = 0$, $t = 0$. (a) Magnitudes and (b) Phases.

gle q and by implementing the nested loop procedure for the observation and source triangles p and q. Ordinary and attachment basis functions are handled in the same way due to introducing appropriate arrays for the corresponding factors and the parameter n inherent in the definition of the different basis functions for each triangle and vertex. The integrals are then included in the impedance matrix and in the excitation vector, if the first part of the attachment basis function is used as the source of the incident field.

The introduction of normalized area coordinates, as in [17], yields an effective procedure for the calculation of the potentials (22) and (23). The resulting integrals may be used for the different basis functions defined on the source triangle q.

V. Results

In order to compare the results of the MPIE method presented in this paper with available measured data, the rect-

angular microstrip spiral inductor with an air-bridge are first chosen [Fig. 1(a)] according to Becks and Wolff [2] as a design example. In contrast to [2], however, the flat strip of the air-bridge may include a finite-metallization thickness t.

For the solution of the MPIE, the MoM with triangular patches (Fig. 2) and basis functions as described in (11) are used. Fig. 2 illustrates the real part of the surface current on the metallic surface of the rectangular microstrip inductor for $f = 11$ GHz. For this example, the lengths of the transmission lines on both sides of the spiral inductors are chosen to be 5 mm, measured from the reference planes (Fig. 1). The imaginary part shows the same behavior for this frequency and is, therefore, not displayed. The structure is excited at port 1.

The results of the two different scattering-matrix extraction techniques, i.e., the MP technique and the CSEV approach, are compared with each other in Fig. 3. For this calculation, the lengths of the transmission lines are first assumed to be 10 mm [Fig. 3(a) and (b)]. Merely at a few frequency points, the MP technique shows some small spikes which depend on the number of considered signal poles and on the number of sampling points. In general, the differences between the two techniques are negligible. However, if the lengths of the lines are reduced (to 5 mm, for example), more significant differences may be perceived [Fig. 3(c)]. It turns out that only the CSEV approach gives accurate results for very short lines. For all following figures, the CSEV approach has, therefore, been used for the extraction of the scattering parameters.

Fig. 4(a) and (b) show the magnitude and phase of the scattering parameter S_{11} of the rectangular spiral inductor of Fig. 1(a) for $t = 0$. Because of some differences to Becks and Wolff [2] for the phases, the authors have used their own FDTD reference calculations. Good agreement between the MPIE calculations and the reference values may be stated. The calculations have been carried out on an IBM RISC 6000 workstation.

In order to demonstrate the influence of a finite air-bridge metallization thickness on the results, Fig. 5 presents the magnitudes and phases of the scattering parameters of the rectangular spiral inductor [Fig. 1(a)] for different metallization thicknesses t. As may be stated, the thickness is of perceptible influence on both the magnitude and phase.

The flexibility of the presented MPIE method is demonstrated by the example of the continuous spiral inductor structure Fig. 1(b). The corresponding scattering parameters are shown in Fig. 6(a) and (b).

VI. Conclusion

The modified space-domain method described in this paper is a powerful and flexible tool to calculate the full-wave scattering parameters of arbitrary 3-D microstrip structures on uniaxial anisotropic layered substrates, including the finite-metallization thicknesses of air-bridges. The method involves mutual coupling effects and losses due to radiation and surface waves. The electromagnetic (EM) fields are described in terms of a flexible MPIE formulation, and the efficient MP and eigenvalue techniques, respectively, are employed to extract the scattering parameters of the circuit under consideration. A triangular mesh allows the convenient modeling of arbitrarily shaped structures without special attachment basis functions. Therefore, the main advantage of this method is its generality, which allows a large variety of printed circuit structures to be characterized with high accuracy and efficiency.

Appendix

A. Definition of the Sommerfeld Integral

$$\mathcal{S}_n\{\tilde{f}(k_\varrho)\} = \frac{1}{2\pi}\int_C \tilde{f}(k_\varrho) J_n(k_\varrho \varrho) k_\varrho^{n+1}\, dk_\varrho \tag{24}$$

where C is a path from 0 to ∞, as discussed in Section III-B.

B. Summary of Transmission-Line Green's Functions

The characteristic admittance and impedance in Felsen's notation [3] are for E-waves

$$Y_i' = \frac{j\omega\epsilon_{\rm t}^i}{jk_z'^i} = \frac{1}{Z_i'} \tag{25}$$

and for H-waves

$$Y_i'' = \frac{jk_z''^i}{j\omega\mu_{\rm t}^i} = \frac{1}{Z_i''} \tag{26}$$

with the vertical propagation constants

$$jk_z'^i = \sqrt{\frac{\epsilon_{\rm rt}^i}{\epsilon_{{\rm r}z}^i}\, k_\varrho^2 - k_0^2 \epsilon_{\rm rt}^i \mu_{\rm rt}^i} \tag{27}$$

$$jk_z''^i = \sqrt{\frac{\mu_{\rm rt}^i}{\mu_{{\rm r}z}^i}\, k_\varrho^2 - k_0^2 \epsilon_{\rm rt}^i \mu_{\rm rt}^i} \tag{28}$$

for E- and H-waves in the ith layer.

The reflection coefficients Γ for E- and H-waves[4] in forward and backward direction are

$$\overrightarrow{\overleftarrow{\Gamma}}_i = \frac{Y_i - \overrightarrow{\overleftarrow{Y}}_i}{Y_i + \overrightarrow{\overleftarrow{Y}}_i} \tag{29}$$

in the ith layer. The $\overrightarrow{\overleftarrow{Y}}_i$ are the terminal admittances at the lower and upper interfaces in the ith layer, corresponding to the

[4] For convenience, the corresponding distinguishing superscripts, $'$ and $''$ (cf. Section II-B), are omitted in the remainder of this section.

left-hand side (LHS) and RHS of the equivalent transmission-line section i at z_i and z_{i+1}.

If the source and observation points are in the same layer $i = j$, the voltage transmission-line Green's function $Z(z, z')$ is

$$Z(z, z') = \frac{e^{-jk_z^i|z-z'|}}{2Y_i(1 - \overleftarrow{\Gamma}_i\overrightarrow{\Gamma}_i e^{-j2k_z^i h_i})}\left[1 + \overleftarrow{\Gamma}_i e^{-j2k_z^i(z_< - z_i)}\right] \cdot \left[1 + \overrightarrow{\Gamma}_i e^{-j2k_z^i(z_{i+1} - z_>)}\right] \tag{30}$$

with $z_< = \min(z, z')$, $z_> = \max(z, z')$, and $h_i = z_{i+1} - z_i$. In these equations, the e-functions have decreasing magnitudes [11].

If observation and source points are in different sections i and j, one has for $z > z'$

$$Z(z, z') = Z(z_i, z')\frac{e^{-jk_z^i(z - z_i)}}{1 + \overrightarrow{\Gamma}_i e^{-j2k_z^i h_i}} \cdot \left[1 + \overrightarrow{\Gamma}_i e^{-j2k_z^i(z_{i+1} - z)}\right] \tag{31}$$

and for $z < z'$

$$Z(z, z') = Z(z_{i+1}, z')\frac{e^{-jk_z^i(z_{i+1} - z)}}{1 + \overleftarrow{\Gamma}_i e^{-j2k_z^i h_i}} \cdot \left[1 + \overleftarrow{\Gamma}_i e^{-j2k_z^i(z - z_i)}\right]. \tag{32}$$

The current transmission-line Green's function $Y(z, z')$ is analogously obtained and may be formulated by interchanging

$$\overleftarrow{\Gamma}_i \to -\overrightarrow{\Gamma}_i$$
$$Y_i \to Z_i$$
$$Z_i \to Y_i$$
$$Z(z, z') \to Y(z, z')$$

in the preceding equations. The remaining transmission-line Green's functions $T(z, z')$ are determined by using the equations

$$-\frac{d}{dz}Y(z, z') = jk_z^i Y_i T^V(z, z') \tag{33}$$

and

$$-\frac{d}{dz}Z(z, z') = jk_z^i Z_i T^I(z, z') \tag{34}$$

given in [3].

The authors thank J. Ritter for the FDTD reference calculations, I. D. Rullhusen for many helpful discussions, and J. R. Shewchuk for his mesh generator.

REFERENCES

[1] M. Abramowitz and I. A. Stegun, *Pocketbook of Mathematical Functions.* Thunund Frankfurt/Main, Germany: Verlag Harri Deutsch, 1984.

[2] T. Becks and I. Wolff, "Analysis of 3-D metallization structures by a full-wave spectral domain technique," *IEEE Trans. Microwave Theory Tech.,* vol. 40, pp. 2219–2227, Dec. 1992.

[3] L. B. Felsen and N. Marcuvitz, *Radiation and Scattering of Waves.* Piscataway, NJ: IEEE Press, 1994.

[4] I. S. Gradstein and I. M. Ryshik, *Summen- Produkt- und Integraltafeln.* Thun und Frankfurt/Main, Germany: Verlag Harri Deutsch, 1981.

[5] P. C. Hammer, O. P. Marlowe, and A. H. Stroud, "Numerical integration over simplexes and cones," *Math. Tables Aids Comp.,* vol. 10, pp. 130–137, 1956.

[6] C.-I. G. Hsu, R. F. Harrington, K. A. Michalski, and D. Zheng, "Analysis of multiconductor transmission lines of arbitrary cross section in multilayered uniaxial media," *IEEE Trans. Microwave Theory Tech.,* vol. 41, pp. 70–78, Jan. 1993.

[7] Y. Hua and T. K. Sarkar, "Matrix pencil method for estimating parameters of exponentially damped/undamped sinusoids in noise," *IEEE Trans. Acoust., Speech, Signal Processing,* vol. 38, pp. 814–824, May 1990.

[8] ——, "On SVD for estimating generalized eigenvalues of singular matrix pencil in noise," *IEEE Trans. Acoust., Speech, Signal Processing,* vol. 39, pp. 892–900, Apr. 1990.

[9] M. Kahrizi, T. K. Sarkar, and Z. A. Maricevic, "Space domain approach for the analysis of printed circuits," *IEEE Trans. Microwave Theory Tech.,* vol. 42, pp. 450–457, Mar. 1994.

[10] P. Mezzanotte, M. Mongiardo, L. Roselli, R. Sorrentino, and W. Heinrich, "Analysis of packaged microwave integrated circuits by FDTD," *IEEE Trans. Microwave Theory Tech.,* vol. 42, pp. 1796–1801, Sept. 1994.

[11] K. A. Michalski, "Formulation of mixed-potential integral equations for arbitrary shaped microstrip structures with uniaxial substrates," *J. Electromagnetic Waves Applicat.,* vol. 7, no. 7, pp. 899–917, 1993.

[12] K. A. Michalski and D. Zheng, "Electromagnetic scattering and radiation by surfaces of arbitrary shape in layered media, Part I: Theory," *IEEE Trans. Antennas Propagat.,* vol. 38, pp. 335–344, Mar. 1990.

[13] ——, "Electromagnetic scattering and radiation by surfaces of arbitrary shape in layered media, Part II: Implementation and results for contiguous half-spaces," *IEEE Trans. Antennas Propagat.,* vol. 38, pp. 345–352, Mar. 1990.

[14] J. R. Mosig and F. E. Gardiol, "Analytical and numerical techniques in the Green's function treatment of microstrip antennas and scatterers," *Proc. Inst. Elect. Eng.,* pt. H, no. 2, pp. 175–182, Mar. 1983.

[15] J. R. Mosig and T. K. Sarkar, "Comparison of quasi-static and exact electromagnetic fields from a horizontal electric dipole above a lossy dielectric backed by an imperfect ground plane," *IEEE Trans. Microwave Theory Tech.,* vol. MTT-34, pp. 379–387, Apr. 1986.

[16] F. Olyslager, D. De Zutter, and K. Blomme, "Rigorous analysis of the propagation characteristics of general lossless and lossy multiconductor transmission lines in multilayered media," *IEEE Trans. Microwave Theory Tech.,* vol. 41, pp. 79–88, Jan. 1993.

[17] S. M. Rao, D. R. Wilton, and A. W. Glisson, "Electromagnetic scattering by surfaces of arbitrary shape," *IEEE Trans. Antennas Propagat.,* vol. AP-30, pp. 409–418, May 1982.

[18] A. Sommerfeld, *Vorlesungen über Theoretische Physik, Band VI, Partielle Differentialgleichungen der Physik.* Thun und Frankfurt/Main, Germany: Verlag Harri Deutsch, 1992.

[19] R. Sorrentino, F. Allesandri, M. Mongiardo, G. Avitabile, and L. Roselli, "Full-wave modeling of via-hole grounds in microstrip by three-dimensional mode-matching technique," *IEEE Trans. Microwave Theory Tech.,* vol. 40, pp. 2228–2234, Dec. 1992.

[20] D. R. Wilton, S. M. Rao, A. W. Glisson, D. H. Schaubert, O. M. AL-Bundak, and C. M. Butler, "Potential integrals for uniform and linear source distributions on polygonal and polyhedral domains," *IEEE Trans. Antennas Propagat.,* vol. AP-32, pp. 276–281, Mar. 1984.

[21] J.-G. Yook, N. I. Dib, and L. P. B. Katehi, "Characterization of high frequency interconnects using finite difference time domain and finite element methods," *IEEE Trans. Microwave Theory Tech.,* vol. 42, pp. 1727–1736, Sept. 1994.

[22] D. Zheng and K. A. Michalski, "Analysis of coaxially fed antennas of arbitrary shape with thick substrates," *J. Electromagnetic Waves Applicat.,* vol. 5, no. 12, pp. 1303–1327, 1991.

Rainer Bunger (M'93) received the Dipl.-Ing. degree from the University of Bremen, Bremen, Germany, in 1992, and since that time, has been continued there, working toward the Dr.-Ing. degree in electrical engineering.

His research interests include the solution of field problems of horn antennas, microstrip structures, MMIC's, and scattering structures using moment methods.

Fritz Arndt (SM'83–F'93) received the Dipl.-Ing., Dr.-Ing., and Habilitation degrees from the Technical University of Darmstadt, Darmstadt, Germany, in 1963, 1968, and 1972, respectively.

From 1963 to 1972, he worked on directional couplers and microstrip techniques at the Technical University of Darmstadt. Since 1972, he has been a Professor and Head of the Microwave Department at the University of Bremen, Bremen, Germany. His research activities are in the area of the solution of field problems of waveguide, finline, and optical waveguide structures, antenna design, and of scattering structures.

Dr. Arndt is a member of the VDE and NTG (Germany). He received the NTG Award in 1970, the A. F. Bulgin Award (together with three co-authors) from the Institution of Radio and Electronic Engineers in 1983, and the Best Paper Award of the Antenna Conference JINA 1986 (France).